



## Synthesis and comparison of spent caustic wastewater photocatalytic treatment efficiency with zinc oxide composite

Amin Ahmadpour<sup>a</sup>, Ali Haghghi Asl<sup>a,\*</sup>, Narges Fallah<sup>b</sup>

<sup>a</sup>Faculty of Chemical, Gas and Petroleum Engineering, Semnan University, Semnan, Iran, emails: ahaghghi@semnan.ac.ir (A. Haghghi Asl), aminahmadpour@semnan.ac.ir (A. Ahmadpour)

<sup>b</sup>Chemical Engineering Department, Amirkabir University of Technology, Tehran, Iran, email: nfallah2001@aut.ac.ir

Received 19 December 2016; Accepted 29 September 2017

### ABSTRACT

In this research, the photocatalytic process is used for the treatment of spent caustic wastewater from petrochemical industries. For this purpose, by use of two types of synthetic photocatalyst (synthetic zinc oxide (ZnO-Syn) and combined (composite) zinc oxide with Fe (ZnO-Fe<sub>3</sub>O<sub>4</sub>)) in a photoreactor, and measuring removal percentage of chemical oxygen demand (COD), results are modeled with the design of experiment (DOE) and artificial neural network (ANN) methods. According to the implemented calculations, it can be concluded that the ANN is a more suitable method than the DOE in modeling and forecasting the amount of COD. Modeling of this research showed that increasing the concentration of ZnO-Fe<sub>3</sub>O<sub>4</sub> and ZnO-Syn photocatalyst in a state of neutral pH, in optimal amount of 1.08 and 1.29 g/L, leads to enhance the COD removal up to 88% and 74% without restrictions, respectively, and also 2 g/L for both of them with restrictions leads to 80% and 69% removal efficiency, respectively. In addition, the study of the parameters' effects, including oxidizer amount, aeration rate, pH and the amount of loaded catalyst, indicate that all factors except pH have had positive effect on the model. Also, photocatalyst acidic pH is more suitable at low concentrations of the photocatalyst. Besides that, by increasing pH, the efficiency of removal will be reduced when oxidant is at its low level. The results showed that photolysis and adsorption adoptions have a very small effect on efficiency of COD removal compared with the photocatalyst adoptions and it is negligible. In addition, the photocatalytic method has an acceptable capability for removing phenol in wastewater samples, whereas it is inefficient for reducing the sulfide solution in wastewater.

**Keywords:** Photocatalytic process; Spent caustic wastewater; Artificial neural network; Design of experiment; Chemical oxygen demand

### 1. Introduction

In olefin units of the petrochemical industry, the exhaust gases from the furnace contain the sulfur compounds which are separated in flash drum (distillation column) by using the caustic solution of the olefin, hydrogen and methane materials. In fact, the output caustic solution contains the sulfur materials and it is considered as the spent caustic wastewater that must be disposed from the unit by a suitable treatment. In the process, following the removal of hydrogen sulfide,

the toxic and harmful composition of the sodium sulfide is observed in the output wastewater of the unit. The waste caustic is known as hazardous wastewater because it has high acidity and sulfide, hydrocarbons, sodium-free and inorganic salt compounds. Caustic sodium should be filtered because microorganisms are poisoned by the high concentrations of sulfide in the biological wastewater treatment [1]. Given that, the spent caustic wastewater contains a wide range of hydrocarbons, thus, selecting the photocatalytic oxidation method can be rational and effective for the primary degradation of pollutants before biological treatment and after physical pretreatment. The sulfide pollution is toxic and

\* Corresponding author.

highly corrosive and it damages the equipment. If the sulfide pollution is dissolved into the produced wastewater, it will cause generation of insoluble metal deposits. By using the photocatalytic oxidation method with the oxidizer's materials such as oxygen or hydrogen peroxide, the sulfide and sulfide compounds and hydrocarbon compounds could be oxidized and brought down to the specified standards.

Photocatalytic degradation of these compounds depends on the type and composition of the catalyst, light intensity, the concentration of the raw material, the amount of catalyst, pH of reaction solution, utilizing the method of catalyst and calcination temperature. Determining the effect of the various factors on the photocatalytic efficiency is so important for designing industrial scale treatment process [2]. So far, several studies have been done on spent caustic wastewater treatment.

Carlos and Maugans [3] studied the caustic wastewater treatment by using the wet air oxidation method. They decreased the amount of chemical oxygen demand (COD) from 72,000 to 15,000 mg/L by using 0.2 m<sup>3</sup> of caustic wastewater and diluting it with 0.4 m<sup>3</sup> of water at 260°C and a pressure of 90 bar. Sheu and Weng [4] removed successfully more than 94% COD from the wastewater by using the combination of neutralization and Fenton's reagent process. The study showed that this process has the ability to reduce the COD from 40,000 to 1,400 mg/L and also reducing the sulfides from 19,000 to 1,400 mg/L. In addition, adding the Fenton process to the above sequence leads to reduce more COD, up to 150 mg/L. Rodriguez et al. [5] reported the spent caustic wastewater treatment by using the electro-generated Fenton's reagent. They also reported in their research; the COD removal of 95% at the pH of 4 and the temperature of 40°C by using 100 mg/L of Fe. Nuñez et al. [6] treated the spent caustic wastewater by using the electrochemical oxidation process and removed successfully 93% of COD. Yu et al. [7] reported 68% of COD removal by using the combination process of UV/H<sub>2</sub>O<sub>2</sub> beside to UV/H<sub>2</sub>O<sub>2</sub>/O<sub>3</sub> in the treatment of the spent caustic process. In this study, the process of UV/H<sub>2</sub>O<sub>2</sub> had an efficiency of 44% in COD removal. Hawari et al. [8] studied the caustic wastewater treatment in various processes. They reported 99% of sulfide removal at pH of 5.1 and 98% of COD removal was also observed in this study. It was also reported that oxidation through H<sub>2</sub>O<sub>2</sub> is able to remove 89% of COD at pH of 2.5 and consumption of 19 mol/L of the hydrogen peroxide. Shy Sayid et al. [9] investigated the synthetic spent caustic wastewater treatment by using photo-Fenton oxidation process. They reported 92% of COD removal and 98% of decreasing the sulfide in the optimal conditions. Chen [10] examined the genuine spent caustic wastewater treatment with COD equal to 25,000 by the conventional wet air oxidation methods and catalytic wet air oxidation and reported the reduction of 75% and 95% for the conventional and catalytic method, respectively. Alaiezadeh [11] studied COD reduction of the spent caustic wastewater treatment of the South Pars gas refinery by using the electrical coagulation method. The most efficiency of the process (91%) was carried out at the effective time of 105 min by diluting the wastewater to the water volume ratio of 2, pH of 9, the current density of 62.8 mA/cm<sup>2</sup> and 1.32 g/L of FeSO<sub>4</sub> material.

In photocatalytic systems, the various parameters such as temperature, pH and amount of catalyst and so on impact the efficiency of photocatalytic degradation process. Usually existence of the different factors to examine the photocatalytic reactions leads to increase the number of which causes high cost and needs great time. In order to evaluate the effect of these factors on the efficiency, it is attempted for converting the process of the experiments to a regular plan and regulating the obtained data to reduce the number of the necessary experiments as much as possible, so that, the total of these factors can optimize the plan. For this purpose, the use of design of experiment (DOE) can be an appropriate option. For performing the DOE, among the common designs that are known as the response surface methodology (RSM), it can be noted to the two renowned designs; central composite design and Box–Behnken design (BBD) [12].

Studies show that the artificial neural network (ANN) modeling has not been used for removal or reduction the spent caustic wastewater of COD until now. The ANN is a model for data processing that is made like the human brain by imitation of the biological neural networks. The key element of this model is the new structure of the data processing system that has been formed by a large number of elements (neurons) with internal and strong communications that work harmoniously together to solve specific problems. ANNs transfer the hidden knowledge or rules of further these data to the networking structure by processing of the experimental data that it is said as the learning operation. In general, the learning ability is the most important feature of an intelligent system. A system that can learn is more flexible and its programming will be easier, so that such a system can be better responsive about the new issues and equations. The algorithmic methods are not suitable for implementing these features in machines; as a result, the methods should be based on the same biological models. The data structure is designed and can act as neurons in these networks by helping the programming knowledge, and this data structure is called node. Then, the network is trained by creating a network between these nodes and applies a learning algorithm [13].

Although titanium dioxide has been studied more than any other semiconductor, however, due to its high price and economically non-viability on a large scale, it is not appropriate. In fact, zinc oxide usually is a better case rather than titanium dioxide and leads to higher efficiency [14–16]. The biggest advantage of zinc oxide over titanium dioxide is that it can absorb a greater percentage of the solar spectrum by similar band gap and photocatalytic degradation mechanism. In recent years, this material has received more consideration due to its non-toxicity, more stability and presenting in more active places [17–20]. High stability, high melting point with valuable physical characteristics such as high specific surface area, high pore volume, low cost and non-toxicity, have brought zinc oxide (ZnO) much attraction of scientists for catalytic applications, chemical adsorbents, additives and polymer fillers, anti-wear additives in oil and advanced ceramics [21–23].

The application of ultraviolet light to destroy contaminants by photocatalyst has been considered as a limitation on the industry which should be destroyed by reducing the band gap. For this purpose, there are two methods: a change in physical properties such as particle size and morphology and the other doping with non-metals and different

semiconductors. Various researches have been done in this area that some of them are mentioned consequently [24–27].

## 2. Materials and methods

### 2.1. Sample characteristics

The output of the neutralization segment of the spent caustic wastewater in the olefin unit of the petrochemical industry is selected as the input wastewater sample into the photoreactor. The characteristics of the wastewater are shown in Table 1.

### 2.2. Synthesis of ZnO

For the synthesis of zinc oxide (ZnO) used in this study, precipitation synthesis method using ultrasonic irradiation was implemented [28]. In this experiment, 11 g of zinc acetate are poured into 100 mL of ammonia at ambient temperature, then 4 g of sodium hydroxide are added. Now fill the ultrasonic device with water and plug it in. Pour the prepared solution in several special containers and place it into the centrifuge machine, put the containers into the ultrasonic device carefully and leave it for 60 min to receive its required energy. After this time, bring out the containers and put them in centrifuge machine at 4,000 rpm for 5 min so that nanoparticles formed as colloidal in the solution are fully settled and are separated from the solution. Then, skim the above liquid from containers and wash the nanoparticles with distilled water again. For this, fill the containers with equal amounts of distilled water and then place them in the ultrasonic device to the extent that nanoparticles are fully colloidal in water and are settled once again, then centrifuge them to dissolve the non-nanoparticles. Finally, nanoparticles are settled again. Now skim the liquid on top of the container and repeat this. In the end, place participated white particles in the oven for 24 h at the temperature of 60°C so that the particles are dried completely.

#### 2.2.1. XRD analysis

The structure of synthesized ZnO nanoparticles with X-ray diffraction (XRD) analysis is shown in Fig. 1. As can be seen, the peaks of this pattern well correspond with commercial ZnO peaks and reference model peaks (JCPDS Cards 036-1451) which are the reason for the absence of impurities in the synthesized compounds (index peaks 004, 201, 112, 200, 103, 110, 102, 101, 002, 100). Using the Scherrer equation, particles size of 40 nm was determined [29].

Table 1  
Characteristics of the wastewater used as reactor feed

Characteristic	Amount
COD, ppm	1,280
Biochemical oxygen demand, ppm	615
pH	7.3
Phenol, ppm	4.7
Total dissolved solids, ppm	89,000
Sulfide, ppm	7.8

### 2.2.2. SEM and TEM analysis

As we know, the minimum time required for forming nanoparticles of zinc oxide in ultrasonic irradiation method is 7 min and as time goes higher than 7 min, particle sizes increase in a clear trend [30]. Thus, referring to the required particle size, ultrasound irradiation time can be adjusted.

The image of ZnO nanoparticles with scanning electron microscopic (SEM) and transmission electron microscopic (TEM) analysis is shown in Figs. 2 and 3, respectively. In these figures, the dominant pattern of particle geometry is cauliflower and bars pattern. In this test, the average particle size of the synthetic photocatalyst calculated by Microstructure Measurement software shows the number of 43.6 nm.

### 2.3. Synthesis of ZnO–Fe<sub>3</sub>O<sub>4</sub>

A problem with the use of small particles in nanoscale is the need for separation processes such as centrifugation after

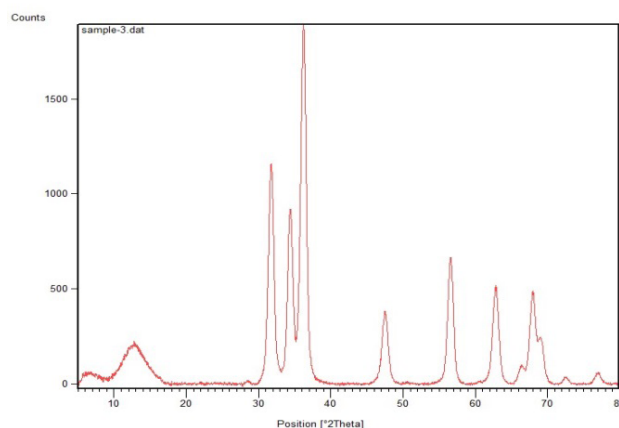


Fig. 1. XRD of ZnO.

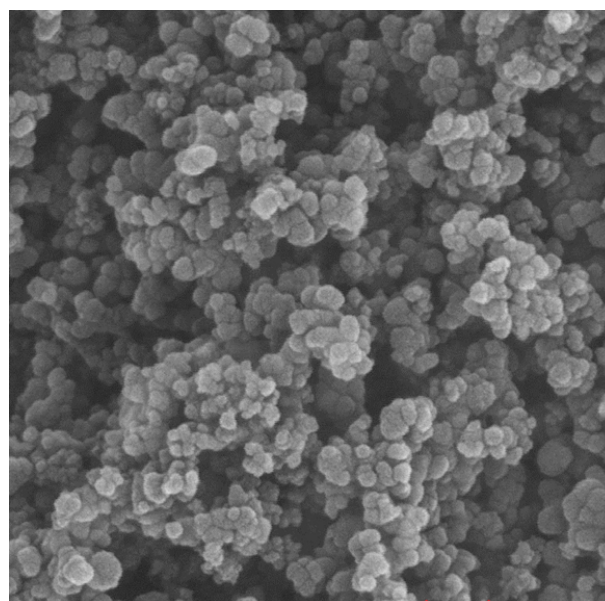


Fig. 2. SEM of ZnO.

use. To solve this problem, the new structure can be built based on the magnetic properties of catalytic Fe particles and use it to decomposition of pollutants. This catalyst consists of a core of  $\text{Fe}_3\text{O}_4$  (magnetite) with magnetic properties and a shell made of zinc oxide. Although zinc oxide is used in several studies for photocatalytic degradation, but catalyst  $\text{ZnO-Fe}_3\text{O}_4$  has been given less attention. This combination (composite) has advantages of  $\text{ZnO}$  and  $\text{Fe}_3\text{O}_4$  altogether.  $\text{ZnO}$  has a high potential in optical dispersion, hence it is intended as a shell in this catalyst. Moreover one of the most important features of this catalyst is magnetism of its core, such that catalyst particles can be easily isolated by applying an external field such as a magnet. Thus, a slurry reactor that is more efficient than a stabilized reactor could be used, without any need for secondary separation steps, such as a centrifuge.

In this research, in order to make zinc oxide photocatalyst combined with  $\text{Fe}^{3+}$ , first photocatalyst  $\text{Fe}_3\text{O}_4$  is synthesized from the salt solutions precipitation method in the aquatic environment. In this method, by adding ammonia to a mixture of ferric chloride of 0.5 M and ferrous sulfate of 0.5 M with a molar ratio of 1/1.75 in the presence of argon as an inert gas, then pH is adjusted to 9. After stirring the solution for 30 min, the participated segment with the magnet is washed by deionized water to reach pH equal to 7 [28].

Now, for modification process, 4 g of obtained  $\text{Fe}_3\text{O}_4$  and 200 mL of 0.5 M sodium nitrate are placed in the ultrasonic device for 20 min and then is stirred for 12 h in the presence of argon gas at a temperature of  $60^\circ\text{C}$ . In the end, the collected particles are washed with acetone.

Core/shell nanoparticles of  $\text{Fe}_3\text{O}_4/\text{ZnO}$  are obtained from the coating of magnetic nanoparticles of  $\text{Fe}_3\text{O}_4$  by direct precipitation method using zinc acetate and ammonium carbonate. To do this, modified  $\text{Fe}_3\text{O}_4$  is added to 100 mL of deionized water for 20 min in the ultrasonic device until a homogenous solution is achieved. Then, 30 mL of it is taken and poured in a separate container, finally the  $\text{Fe}_3\text{O}_4/\text{ZnO}$  particles with a molar ratio of 1:10 for the Fe oxide to zinc oxide is achieved. Afterward, prepare two solutions by adding 12.16 g of  $\text{ZnAC}_2 \cdot 2\text{H}_2\text{O}$  and 7.6 g of  $(\text{NH}_4)_2\text{CO}_3$  to 100 mL of deionized water. Now add  $\text{Fe}_3\text{O}_4$  drop by drop to each of

the above solutions. Then collected deposits are washed by water, ammonia solution (pH = 9) and ethanol. In a situation that there is no  $\text{Fe}_3\text{O}_4$  in the container,  $\text{ZnO}$  will be formed in the same way. Finally, particles are settled and rinsed, dried in a vacuum for 12 h and are calcined according to designed temperature and time.

### 2.3.1. XRD analysis

X-ray diffraction curve for the modified  $\text{Fe}_3\text{O}_4$ ,  $\text{ZnO}$  and core-shell of  $\text{Fe}_3\text{O}_4/\text{ZnO}$  is shown in Fig. 4. Using Scherrer equation, the particle size of modified  $\text{Fe}_3\text{O}_4$  nanoparticles and  $\text{Fe}_3\text{O}_4/\text{ZnO}$  nanoparticles was calculated as 14 and 51 nm, respectively. Also in spades  $\text{Fe}_3\text{O}_4/\text{ZnO}$ , there is an abrupt increase in some peaks that is due to overlapping of integrated peaks.

### 2.3.2. SEM analysis

Figs. 5 and 6 provide SEM and TEM analysis of obtained nanoparticles. The average particle size of  $\text{Fe}_3\text{O}_4/\text{ZnO}$ , in this case, is obtained about 57 nm. Also in these figures, the identical structure of hybrid nanoparticles of  $\text{Fe}_3\text{O}_4/\text{ZnO}$  is almost confirmed.

$\text{Fe}_3\text{O}_4/\text{ZnO}$  particles in this figure are formed and the particle size varies with that calculated from Scherrer formula which is because of the formation of particles from the accumulation of several crystal systems.

### 2.3.3. FTIR analysis

Fig. 7 shows Fourier-transform infrared spectroscopy (FTIR) for core/shell nanoparticles of  $\text{Fe}_3\text{O}_4/\text{ZnO}$ . In this figure, the absorption spectra for Fe–O bond are observed in 580 and  $620\text{ cm}^{-1}$  and the absorption spectrum for broadband  $\text{OH}^-$  is observed in  $3,450\text{ cm}^{-1}$ .

Furthermore, absorption in  $1,395$  and  $1,590\text{ cm}^{-1}$  area signifies the presence of  $\text{COO-Fe}$  which can be the result of the reaction of hydroxyl radical with carboxyl anion, at  $\text{Fe}_3\text{O}_4$  surface, to increase the amount of sodium citrate. However, the presence of this peak reflects the successful bond of sodium citrate on the surface of  $\text{Fe}_3\text{O}_4$  nanoparticles.

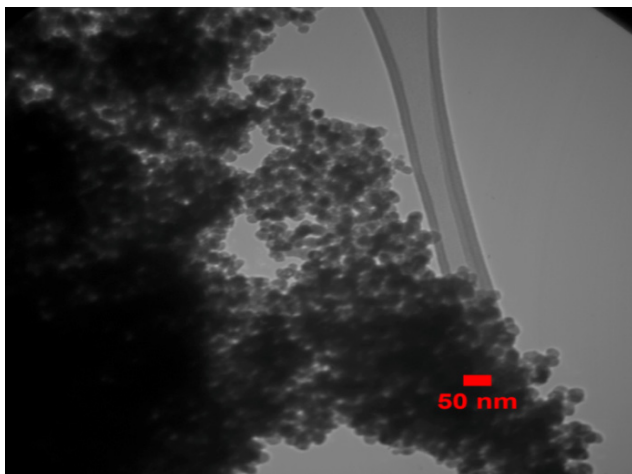


Fig. 3. TEM of  $\text{ZnO}$ .

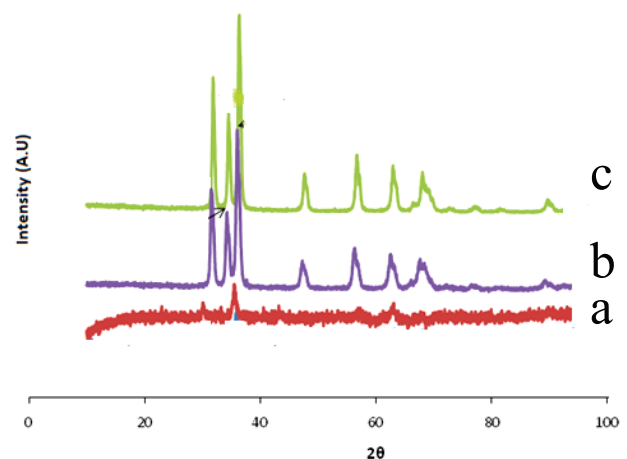
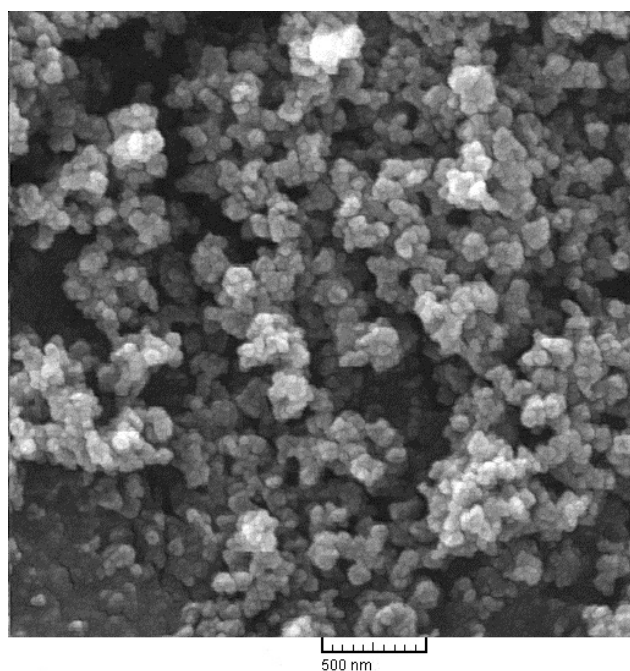
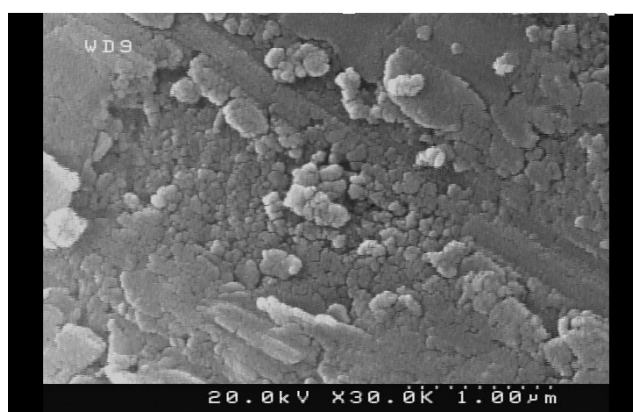
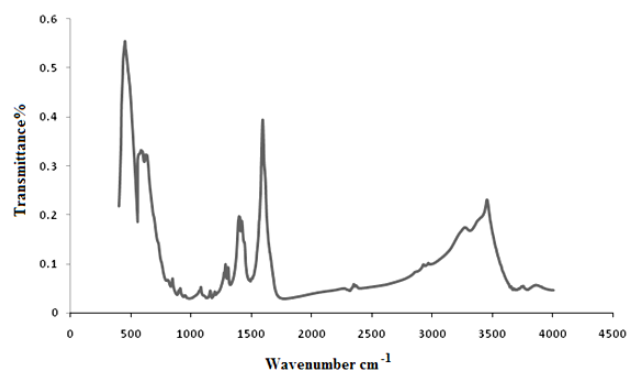


Fig. 4. XRD for (a) modified  $\text{Fe}_3\text{O}_4$ , (b)  $\text{ZnO}$  and (c)  $\text{Fe}_3\text{O}_4/\text{ZnO}$ .

Fig. 5. SEM of Fe<sub>3</sub>O<sub>4</sub>/ZnO.Fig. 6. TEM of Fe<sub>3</sub>O<sub>4</sub>/ZnO.Fig. 7. FTIR of Fe<sub>3</sub>O<sub>4</sub>/ZnO.

Absorption in 450 cm<sup>-1</sup> also indicates the presence of Zn–O bond. From the combination of results of this test with those of XRD test of ZnO, it can be assured that ZnO coating on Fe<sub>3</sub>O<sub>4</sub> is done successfully.

#### 2.4. $pH_{pzc}$ analysis

According to Fig. 8, the  $pH_{pzc}$  (zero charge point pH of photocatalyst which determines the range of adsorption according to the cationic or anionic nature of the wastewater) used for ZnO-Syn and ZnO–Fe<sub>3</sub>O<sub>4</sub> was 8.5 and 6.0, respectively [31].

#### 2.5. Experimental procedures

In this study, all the oxidation reactions have been carried out discontinuous in atmospheric conditions by a double-cylindrical-shell photoreactor with stirrer. The related photocatalyst was used in the photocatalytic degradation process as a sparse manner in a solution (slurry solution). Slurry reactor has a double-cylindrical-shell that it was made by the 304-stainless steel. In this photoreactor, eight 16-W UV-C (for ZnO-Syn) and eight 16-W visible (for ZnO–Fe<sub>3</sub>O<sub>4</sub>) bubble lights (made by Philips Company, Amsterdam, The Netherlands) were used with the eight quartz glass sheath. In fact, for positioning the lamps inside photoreactor, some quartz pipes with the size of 45 × 2 cm were vertically used in the intended places. The distance of lamps from each other should be the same for generating uniform light intensity in the reactor. During the test, an aluminum foil was used on the door of reactor to avoid light emission to the surrounding. The Viton gaskets were also used to block the surrounding of the quartz glass after reactor installation. A blade stirrer with three rows shaped blades was used for stirring the reaction solution and this blade stirrer was equipped with a 12 V DC electromotor with 200 rpm. The required oxygen has been provided via aeration by means of a Heila compressor with the capacity of 35 L/min, and after measuring by a rotameter, the oxygen was injected through an annular aquarium sparger in order to create smaller bubbles and proper distribution of air into the system. The photoreactor was equipped with a jacket cooling water system to control the temperature. The range of recorded temperature is between 26°C and 27°C in all stages of the test that it shows the isothermal reaction conditions. This photoreactor is schematically shown in Fig. 9.

In this study, first, a sample was taken from the reactor before the photocatalytic reaction and its COD value were determined in order to study the effect of photocatalytic reaction during test implementation and comparing it with the adsorption process (absence of light) and photolysis (presence of light). Then, under the determined conditions by the DOE, during the test (90 min) and at intervals of 10 min, 2 mL of the reactor contents was taken and its COD was determined in the photocatalytic reaction. The lab method (Standard No. 5220 APHA) was used for this purpose. The 5530-D standard APHA laboratory method is used to measure the amount of phenol in the wastewater sample, and the chemical method of the methylene blue is used to determine the amount of dissolved sulfide into the wastewater [32].

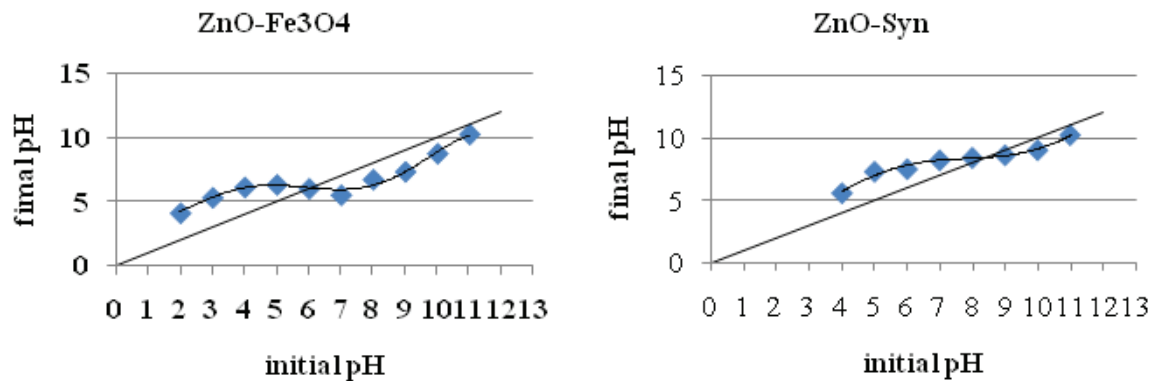


Fig. 8.  $pH_{pzc}$  of ZnO-Syn and ZnO-Fe<sub>3</sub>O<sub>4</sub>.

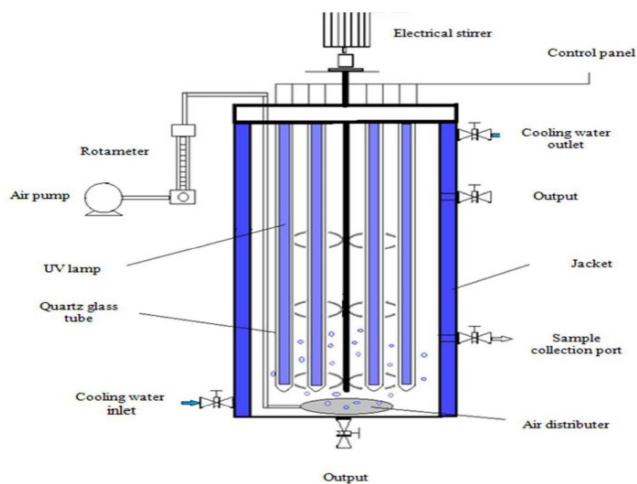


Fig. 9. Schematic of experimental photoreactor.

In this study, the efficiency of photocatalytic removal of COD in the 90th minute was selected as the response (objective function) and it can be calculated by using Eq. (1). In this regard,  $C_0$  and  $C$  are the COD parameters at the beginning of the photocatalytic process (moment of turning on the lamps) and at sampling time of the 90th minute, respectively [33].

$$\text{Degradation efficiency (\%)} = \frac{C_0 - C}{C_0} \times 100 \quad (1)$$

## 2.6. Design of experiment and artificial neural network modeling

The two-level factorial screening method was used. In order to determine the main factors of the photocatalytic process by using ZnO photocatalyst of the research and Design Expert software. Four factors were determined as the main factors: photocatalyst concentration ( $A$ ), pH ( $B$ ), the concentration of auxiliary oxidant (hydrogen peroxide 33 wt%) ( $C$ ) and the aeration rate ( $D$ ). The DOEs (the RSM of the BBD type) were used for modeling (all the analysis was done at 95% level of confidence) [34]. This model is useful for performing the experiments and achieving an appropriate model to investigate important factors of the process [35].

In this method, a polynomial is used according to Eq. (2) for the relationship between response and independent variables. In this regard,  $y$  is the response variable or the percentage of the COD removal,  $\beta_0$  is the constant value of the polynomial,  $\beta$ ,  $\beta_{ii}$ ,  $\beta_{ij}$  are the regression coefficients of interaction,  $x_j$ ,  $x_i$  are the independent variables and  $\varepsilon$  is the random error rate [36].

$$y = \beta_0 + \sum_{i=1}^k \beta_i x_i + \sum_{i=1}^k \beta_{ii} x_i^2 + \sum_{1 \leq i < j \leq k} \beta_{ij} x_i x_j + \varepsilon \quad (2)$$

In this design, under selected operating conditions, 30 tests emerge with repetitive six-point. The aim of the DOE in the present study is the optimization of the removal process of COD in the wastewater sample. Statistical analysis and the proposed model have been provided by a trial version of software Design Expert V.8 (Table 3).

In order to analyze the provided model for each catalyst, analysis of variance (ANOVA) is presented in Tables 4 and 5. Usability and accuracy of the models offered for the amount of COD removal of the photocatalytic processes of ZnO-Syn and ZnO-Fe<sub>3</sub>O<sub>4</sub> are carried out by RSM using parameters  $R^2$ ,  $R^2_{adj}$ ,  $F$  and  $p$  parameters.

In this study, the single layer perceptron (SLP) method for ANN modeling is specifically described for the photocatalytic removal of COD by ZnO-Syn and ZnO-Fe<sub>3</sub>O<sub>4</sub> catalysts. To create the desired model, laboratory data were used for teaching and learning the process of the neural network. A typical structure of the neural network used in this study is shown in Fig. 10. As shown in this figure, ANN includes an input layer, a hidden layer and an output layer. The input variables for the neural network are the amount of catalyst (g/L), pH, oxidant (ppm) and the aeration rate (L/min). The experimental COD removal is output in this structure.

The desired number of hidden layers of neural network model was obtained by changing the number of hidden layers network from 2 to 20 layers, accordingly, the highest COD removal efficiency was achieved. Thus, a series of data are used for confirmation of the reliability of neural network model. With the exception of correction coefficients, which are based on Eq. (3), root mean squared errors (RMSEs), the mean absolute deviation (AAD) and the mean absolute error (MAE) were used to justify the model.

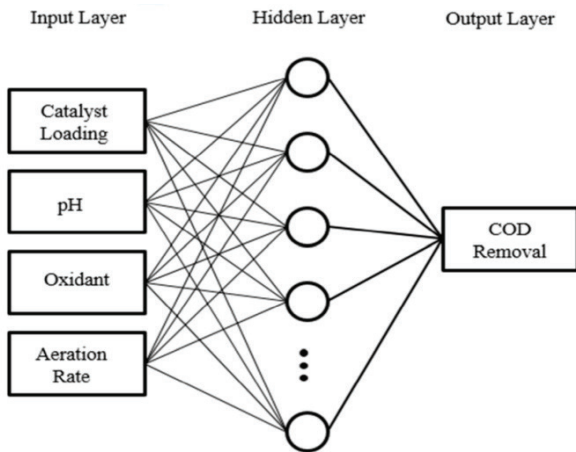


Fig. 10. Structure of designed neural network.

$$R^2_{adj} = 1 - \left[ (1 - R^2) \frac{n-1}{n-K-1} \right] \quad (3)$$

where  $n$  is the number of all trials and  $K$  is the number of independent variables [38]. The model performance characteristics can be explored based on the following equations:

$$RMSE = \sqrt{\frac{\sum_{i=1}^n (X_m - X_p)^2}{n}} \quad (4)$$

$$MAE = \frac{\sum_{i=1}^n |X_m - X_p|}{n} \quad (5)$$

$$AAD = \left\{ \frac{\sum_{i=1}^n (|X_m - X_p| / X_m)}{n} \right\} \times 100 \quad (6)$$

In Eqs. (4)–(6),  $n$  is a number of data points,  $X_m$  is measured objective factor values and  $X_p$  is predicted models. The toolbox of Matlab (windows version) was used to analyze ANN and create an SLP and call levels for objective function (COD removal). Finally, the comparison between DOE and ANN was performed by the following characteristics:  $R^2$ ,  $R^2_{adj}$ , MAE and AAD.

### 3. Results and discussion

#### 3.1. The analysis of DOE

The results of the experiment in different conditions of Table 2 have been collected in Table 3. Both methods of ANN and DOE are an indication of the validity of the results described in the following sections. The results of experiments on both types of catalyst ZnO-Syn and ZnO-Fe<sub>3</sub>O<sub>4</sub> at different process conditions are presented in Table 3.

Table 2  
The levels of selected factors

Factor	Sign	Each variable level code	
		Low	High
Photocatalyst concentration (g/L)	A	-1	+1
pH	B	4	10
Auxiliary oxidant concentration (ppm)	C	0	300
Aerating rate (L/min)	D	0.5	4

#### 3.1.1. Analysis of variance

A matrix based on BBD model with four factors for both ZnO-Fe<sub>3</sub>O<sub>4</sub> and ZnO-Syn catalyst and experimental results in the removal of COD photocatalytic percentage shown in Tables 4 and 5. For each catalyst, a quadratic model is estimated to fit the data based on obtained experimental data. These models can be present separately based on parameter codes to evaluate the performance of both implemented catalysts.

The model is shown in actual parameters shape for ZnO-Syn in Eq. (7):

$$R = -66.611351 + 45.19444 \times A + 18.09732 \times B - 0.11214 \times C + 34.80403 \times D + 4.06975 \times A \times B - 0.087231 \times A \times C + 0.039765 \times B \times C - 0.87074 \times B \times D - 0.048572 \times C \times D - 17.03610 \times A^2 - 1.89366 \times B^2 - 3.540E^{-004} \times C^2 - 5.28564 \times D^2 \quad (7)$$

According to Table 4, we can find  $AD$  term that removed because of unacceptability for statistical purposes, as result.

The accuracy of the model which is a comparison between actual values vs. predicted values is shown in Fig. 11(a). It is obvious from the figure that there is no sensible error in the model. The normal probability distribution of residues clustered graph is shown in Fig. 11(b). This figure is a study key to discovering that error variance is the same or not [37,38].

Also, residue analysis in Fig. 11(c) is presented to the adequacy of the model to which based on that it is obvious the difference between model output values and experimental data are not so much.

The model is shown in actual parameters shape for ZnO-Fe<sub>3</sub>O<sub>4</sub> in Eq. (8):

$$R = -42.55137 + 47.86162 \times A + 5.50458 \times B - 8.85135E^{-004} \times C + 43.52598 \times D + 5.549770 \times A \times B - 0.10396 \times A \times C - 7.44931 \times A \times D + 0.054581 \times B \times C - 0.019081 \times C \times D - 12.16731 \times A^2 - 1.73406 \times B^2 - 2.8324E^{-004} \times C^2 - 5.25817 \times D^2 \quad (8)$$

Table 3  
DOE/ANN results

Run	A: catalyst loading (g/L)	B: pH	C: $C_{H_2O_2}$ (ppm)	D: air (L/min)	COD removal % with ZnO-Syn (experimental)	COD removal % with ZnO-Syn (RSM)	COD removal % with ZnO-Syn (ANN)	COD removal % with ZnO- $Fe_3O_4$ (experimental)	COD removal % with ZnO- $Fe_3O_4$ (RSM)	COD removal % with ZnO- $Fe_3O_4$ (ANN)
1	1.25	7.00	150.00	2.25	73	72	71	75	75	75
2	1.25	7.00	300.00	0.50	30	34	31	67	63	67
3	2.00	10.00	150.00	2.25	62	63	62	73	72	72
4	1.25	7.00	150.00	2.25	67	71	71	76	75	75
5	2.00	7.00	300.00	2.25	71	67	71	84	86	84
6	0.50	10.00	150.00	2.25	15	18	15	12	12	12
7	1.25	10.00	0.00	2.25	20	15	20	10	10	11
8	0.50	7.00	150.00	0.50	22	23	23	12	11	12
9	1.25	7.00	300.00	4.00	73	79	73	86	80	86
10	0.50	7.00	0.00	2.25	12	22	12	14	14	10
11	1.25	4.00	150.00	0.50	19	24	20	46	41	47
12	2.00	7.00	150.00	0.50	58	50	58	68	66	68
13	1.25	7.00	0.00	0.50	50	43	49	10	16	10
14	1.25	7.00	0.00	4.00	42	35	42	49	53	48
15	1.25	7.00	150.00	2.25	71	72	71	69	75	75
16	1.25	7.00	150.00	2.25	75	72	71	77	75	75
17	2.00	7.00	0.00	2.25	59	68	59	70	72	70
18	0.50	7.00	150.00	4.00	49	42	47	58	57	59
19	1.25	10.00	300.00	2.25	73	69	73	86	85	86
20	1.25	4.00	0.00	2.25	61	60	61	72	70	73
21	0.50	4.00	150.00	2.25	49	46	49	58	59	57
22	1.25	4.00	300.00	2.25	42	43	42	50	58	52
23	1.25	10.00	150.00	0.50	31	35	31	13	19	14
24	0.50	7.00	300.00	2.25	63	60	62	75	74	74
25	1.25	10.00	150.00	4.00	33	33	33	39	46	40
26	1.25	4.00	150.00	4.00	60	62	65	71	68	74
27	2.00	7.00	150.00	4.00	64	72	64	75	73	76
28	1.25	7.00	150.00	2.25	68	69	71	75	75	75
29	2.00	4.00	150.00	2.25	59	54	59	79	69	77
30	1.25	7.00	150.00	2.25	77	71	71	79	75	75

Table 4  
Analysis of variance with ZnO-Syn

Source	Sum of squares	df	Mean square	F value	p Value prob > F
Model	11,062.26	13	850.94	18.87	<0.0001 significant
A: catalyst loading	2,188.90	1	2,188.90	48.54	<0.0001
B: pH	266.60	1	266.60	5.91	0.0272
C: C <sub>H<sub>2</sub>O<sub>2</sub></sub>	971.70	1	971.70	21.55	0.0003
D: air	997.25	1	997.25	22.11	0.0002
AB	335.40	1	335.40	7.44	0.0149
AC	385.22	1	385.22	8.54	0.0100
BC	1,280.79	1	1,280.79	28.40	<0.0001
BD	385.84	1	385.84	8.56	0.0099
CD	650.26	1	650.26	14.42	0.0016
A <sup>2</sup>	629.69	1	629.69	13.96	0.0018
B <sup>2</sup>	1,991.73	1	1,991.73	44.17	<0.0001
C <sup>2</sup>	437.26	1	437.26	9.70	0.0067
D <sup>2</sup>	1,796.76	1	1,796.76	39.84	<0.0001
Residual	721.54	16	45.10	–	–
Lack of fit	644.70	11	58.61	3.81	0.0755 not significant
Pure error	76.83	5	15.37	–	–
Corrected total	11,783.80	29	–	–	–

Table 5  
Analysis of variance with ZnO-Fe<sub>3</sub>O<sub>4</sub>

Source	Sum of squares	df	Mean square	F value	p Value prob > F
Model	18,682.23	13	1,437.09	46.26	<0.0001 significant
A: catalyst loading	3,750.48	1	3,750.48	120.74	<0.0001
B: pH	1,488.88	1	1,488.88	47.93	<0.0001
C: C <sub>H<sub>2</sub>O<sub>2</sub></sub>	4,106.41	1	4,106.41	132.20	<0.0001
D: air	2,173.50	1	2,173.50	69.97	<0.0001
AB	612.05	1	612.05	19.70	0.0004
AC	547.18	1	547.18	17.62	0.0007
AD	382.38	1	382.38	12.31	0.0029
BC	2,413.08	1	2,413.08	77.68	<0.0001
CD	100.35	1	100.35	3.23	0.0912
A <sup>2</sup>	321.20	1	321.20	10.34	0.0054
B <sup>2</sup>	1,670.15	1	1,670.15	53.77	<0.0001
C <sup>2</sup>	278.50	1	278.50	8.97	0.0086
D <sup>2</sup>	1,778.13	1	1,778.13	57.24	<0.0001
Residual	497.00	16	31.06	–	–
Lack of fit	440.17	11	40.02	3.52	0.0878 not significant
Pure error	56.83	5	11.37	–	–
Corrected total	19,179.23	29	–	–	–

Importance and competence of model have been tested by ANOVA. The *p* value and *F* value of the model prove the high validity of the model.

According to Table 5, we can find *BD* term that removed because of unacceptability for statistical purposes, as result. Verifying the model charts are shown in Fig. 12.

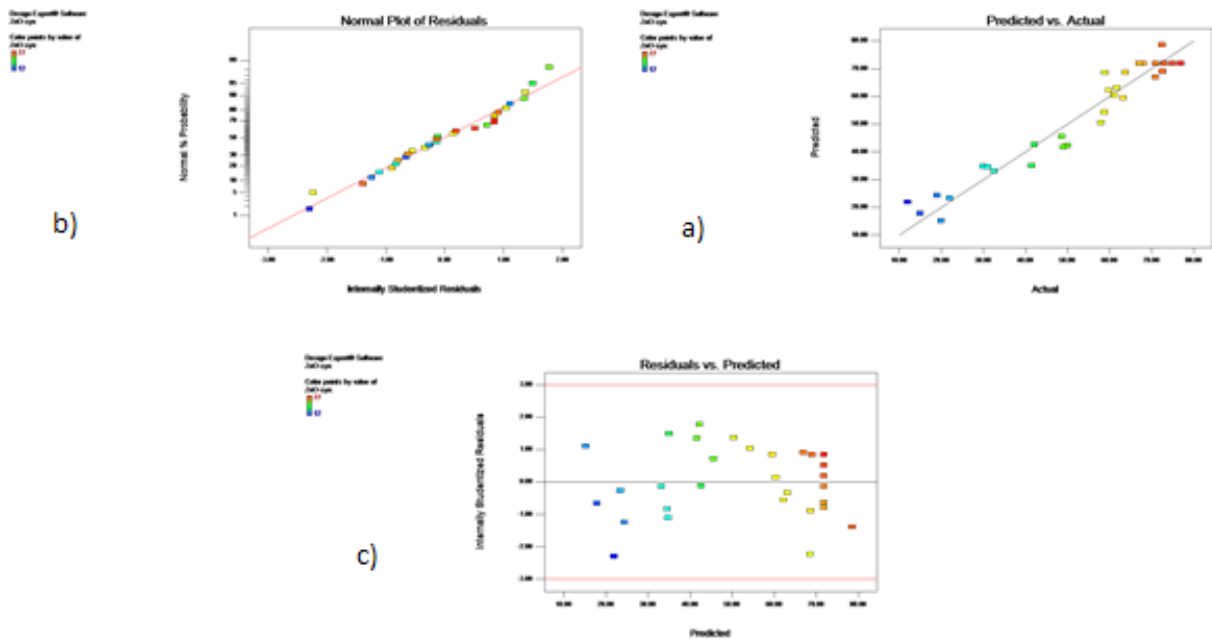


Fig. 11. Verifying the model: (a) predicted vs. actual, (b) normal plot of residuals and (c) residuals vs. predicted for ZnO-Syn.

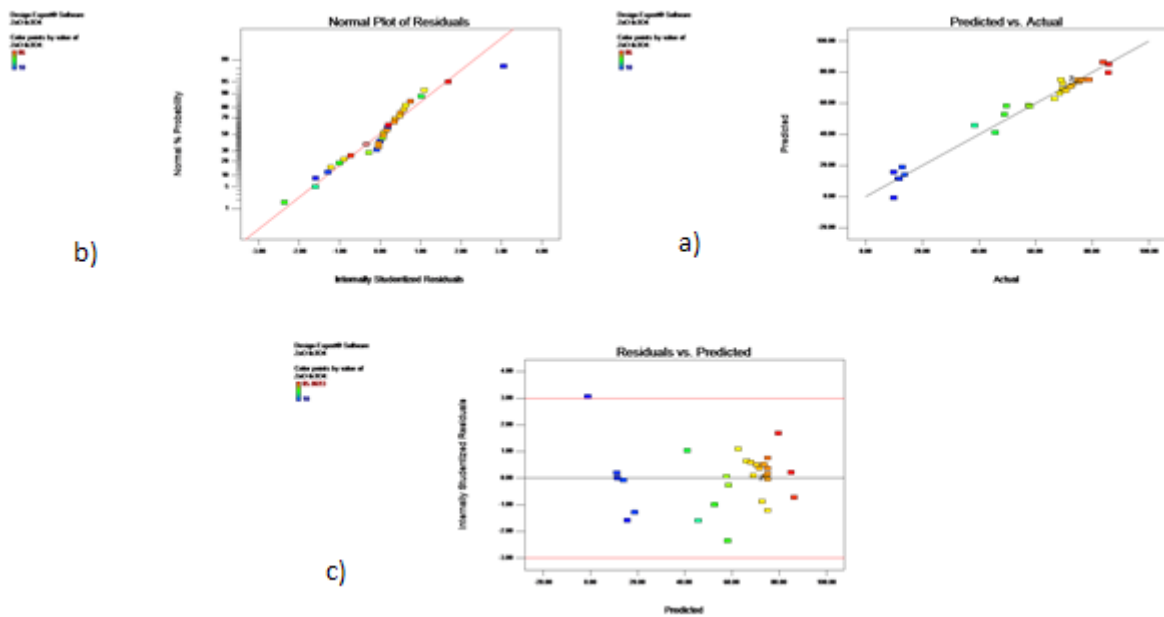


Fig. 12. Verifying the model: (a) predicted vs. actual, (b) normal plot of residuals and (c) residuals vs. predicted for ZnO-Fe<sub>3</sub>O<sub>4</sub>.

### 3.2. Effective parameters study

#### 3.2.1. Interaction effect of photocatalyst quantity and pH

Interaction effect of solvent primary pH and amount of studied catalysts of ZnO-Syn/ZnO-Fe<sub>3</sub>O<sub>4</sub> in three different levels of supporting oxidizing and aeration rate factor mid-level are shown by 3D plots (Fig. 13). As is evident from charts, the high value of oxidizing agent cause maintaining removal at high levels and vice versa.

As we know, generally photocatalytic processes have high efficiency at low pH. So according to related charts, it seems when the oxidizing agent is at its low level, we see decreasing in efficiency as pH is increased, it means pH and oxidizing agent have a reciprocal effect on the process. The interaction between the initial solution pH and the loaded catalyst in the process at three different levels; factor of the auxiliary oxidants rate and mid-level of aeration intensity factor. The higher concentrations of photocatalyst require a

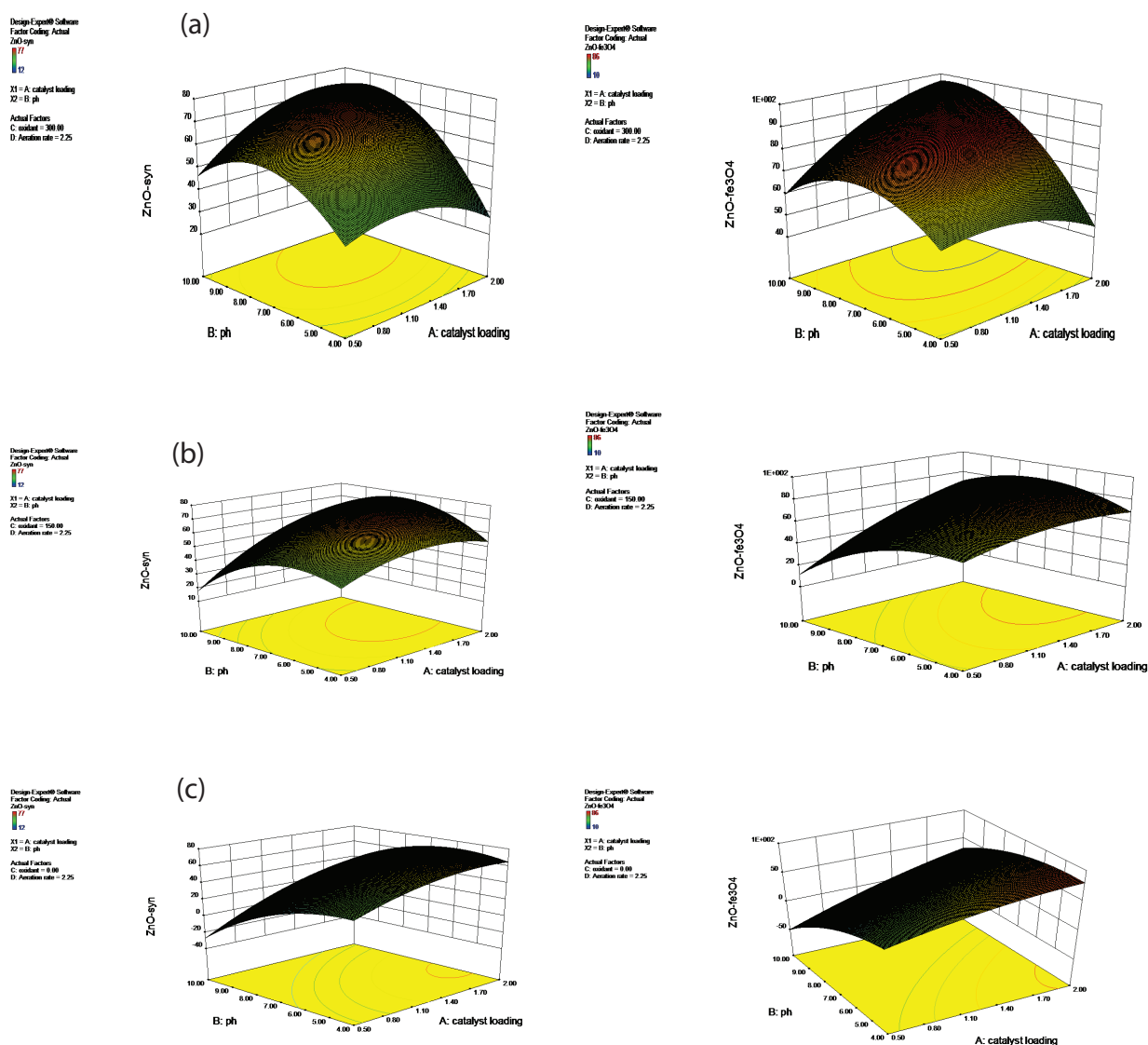


Fig. 13. Three-dimensional graphs of photocatalyst parameter amounts changes, pH at different levels of oxidizer and the average amount of aeration intensity. (a) Maximum amount of oxidizer, (b) average amount of oxidizer and (c) minimum amount of oxidizer.

higher pH to prevent the aggregation. However, the production of hydroxyl radicals depends only on the positive reaction of the hole with the water molecule or hydroxide ions, which shortages of secondary sources for the production of radical hydroxyl (radical hydroperoxyl) is compensated by increasing the amount of photocatalyst. In the alkaline pHs, absorption of pollutants has decreased, therefore, the rate of degradation will be reduced according to the created negative load on the photocatalyst surfaces. pH is one of the parameters that play a fundamental role in the photocatalytic processes. The existence of high levels of antioxidants leads to maintain a great amount of the removal rate. Generally, photocatalytic processes have higher efficiency in low pH. According to the relevant plants, the existence of the antioxidants with high level prevents to emerge high pH effect on the process which means that pH and oxidant have positive interaction in the process. In addition, as pH increases, the efficiency decreases when the oxidant is at a low level.

As shown in the charts of both related catalyst, the adsorption rate is made higher and reversed by large amounts of oxidizing agent. As we know, the generally photocatalytic process has high efficiency at low pH thus, considering related charts it is been seen the existence of oxidizing agent at large amount preventing high pH effect for the process. In another word, oxidizing agent and pH have a positive reciprocal effect on the process. Also, when the oxidizing agent is at a low level, the corresponding pH value increases that would reduce the removal efficiency.

By comparing the performance of the two catalysts, it is shown in Fig. 13(a) that the loading of the ZnO-Fe<sub>3</sub>O<sub>4</sub> catalyst is changing to improve the efficiency of COD removal from ZnO-Syn at low pH and high oxidant levels, which gradually decreases the amount of the agent. The oxidizing agent has been reduced and it is clearly shown that the value of the inverse catalyst is the effect of Fig. 13(c) and the amount of ZnO-Syn catalyst is more effective than Fe<sub>3</sub>O<sub>4</sub>

and the amount of COD removal efficiency in the ZnO-Syn catalyst is higher.

3.2.2. Effectiveness percentage graph of each parameter

It is clear from Fig. 14 that all factors have a positive effect on model (unless pH), which means if we ignore reciprocal effect, efficiency increase as each factor increase.

Effects of all parameter are calculated based on Eq. (9) according to coefficient values in the predicted model.

$$\%P_i = \frac{b_i^2}{\sum b_i^2} \tag{9}$$

where *P* is effectiveness degree percentage of each term and *b* is the coefficient of each model's terms (Eq. (9)). According to this equation, a diagram of each parameter is drowned on the figure. This diagram shows the effectiveness percentage of each parameter, the blue color shows that the terms have a positive effect and red color shows a negative effect of the terms in the model. This diagram clearly shows all major factors unless pH has a positive effect in the model and comparing two (a) and (b) diagrams of Fig. 14, it is obvious that negative effect of pH on the ZnO-Fe<sub>3</sub>O<sub>4</sub> catalyst is more than ZnO-Syn.

According to Fig. 14, increasing effect of each factor in a process involving ZnO-Fe<sub>3</sub>O<sub>4</sub> is more than ZnO-Syn. In all experiments, reciprocal effect of catalyst value and pH (AB) and reciprocal of pH and oxidant (BC) have a positive effect according to Fig. 14(a) interaction between catalyst value and oxidant (AC) and also pH and aeration rate (BD) have negative

effect on model. According to Fig. 14(b), interaction between catalyst value and oxidant (AC) and catalyst value and aeration rate (AD) and also interaction between oxidant and aeration rate (CD) have negative effect on model. Despite of the model involving ZnO-Fe<sub>3</sub>O<sub>4</sub> and ZnO-Syn, the reciprocal effect of oxidant and aeration rate (CD) has a positive effect.

3.3. Optimization of influence parameters in catalysts process

In this study, optimization is discussed in two states: (1) without factor value adjustment which is called optimization without constraint and (2) with factor value adjustment which is called optimization with constraint. In optimization without factor adjustment, all factors are in own ranges and COD removal rate that is the objective function placed at maximum state. The results of this optimization for the model's data associated with the ZnO-Syn catalyst, 80% and for the model's data associated with ZnO-Fe<sub>3</sub>O<sub>4</sub>, 88% are obtained. In optimization with factors adjustment, the pH factor is set on number 7 and we placed the using rate of oxidizer on minimum. As before, COD removal efficiency will be at its maximum. The results of this optimization for the model's data associated with ZnO-Syn catalyst, 69% and for the model's data associated with ZnO-Fe<sub>3</sub>O<sub>4</sub>, 74% are obtained.

3.4. The analysis of ANN

The used neural network in this study is SLP which has been trained as the feedback, so that, only the input layer connects to the hidden layer and the hidden layer connects to the output layer. To select the number of neurons, each

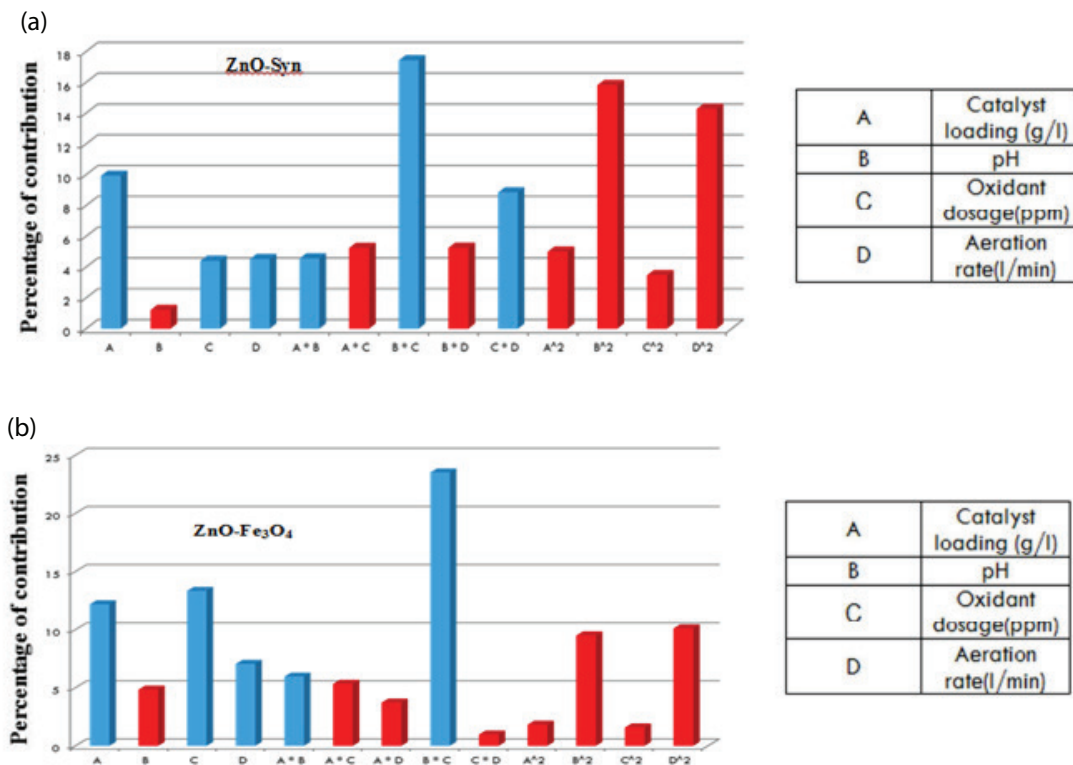


Fig. 14. Effect of each parameter diagram for both catalyst (a) ZnO-Syn and (b) ZnO-Fe<sub>3</sub>O<sub>4</sub>.

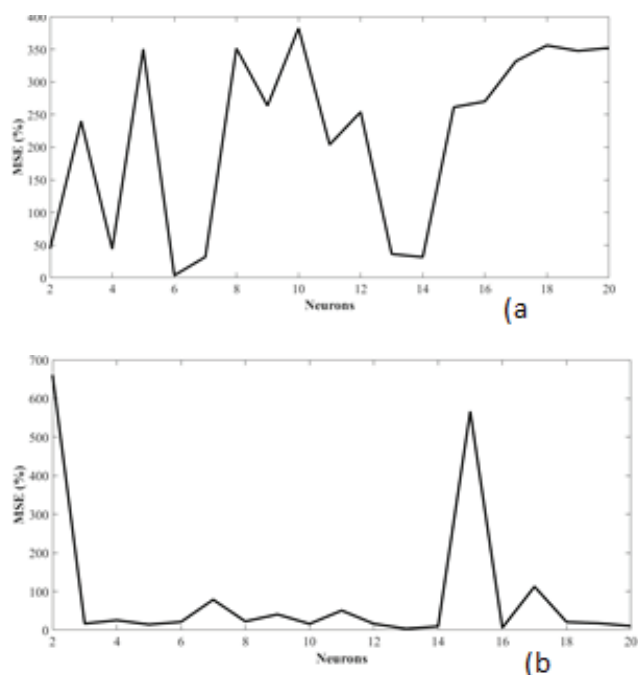


Fig. 15. MSE value for (a) ZnO-Syn and (b) ZnO-Fe<sub>3</sub>O<sub>4</sub>.

time, the number of 2–20 neurons was considered in the hidden layer and the network was trained, then the mean squared error (MSE) value was calculated. The calculated MSE value is shown for each number of neurons in Fig. 15. The number of neurons which has a minimum MSE value is considered as best structure, so according to Fig. 15(a) for network training of ZnO-Syn, 6 neurons and according to Fig. 15(b) for network training of ZnO-Fe<sub>3</sub>O<sub>4</sub>, 13 neurons are used in the hidden layer. Network training for each structure repeated three times to remove random results.

The number of existing input and output data sets available for training the network are 30 which 24 of them were used for training and 6 of them were used for validation and test. In Fig. 16, the diagram of experimental output data vs. results data of network training is shown. As the diagram slope approaches to unity, provided model accuracy would become more and this is true of neural network design. Figs. 16(a) and (b) according to  $R^2$  value show high accuracy of neural network training design.

To compare two methods of experiment design and neural network for the process of ZnO-Syn catalyst it is used two criteria of  $R^2$  and MSE.  $R^2$  value is 0.9388 and 0.9904, respectively, for DOE and ANN and RMSE value is calculated as 0.6814 and 0.3211, respectively, for DOE and ANN. According to results, the ANN is more efficient way than DOE in modeling and predicting COD value (Table 6). Also, to compare two methods of DOE and ANN for the process of ZnO-Fe<sub>3</sub>O<sub>4</sub> catalyst it is used two criteria of  $R^2$  and MSE.  $R^2$  value is 0.9741 and 0.9950, respectively, for DOE and ANN and RMSE value is calculated as 0.4421 and 0.2614, respectively, for DOE and ANN (Table 7). According to results, the ANN is more efficient way than DOE in modeling and predicting of COD value.

Two-dimensional contour plots in Fig. 17 were used to study the effect of the considered parameters on the value of

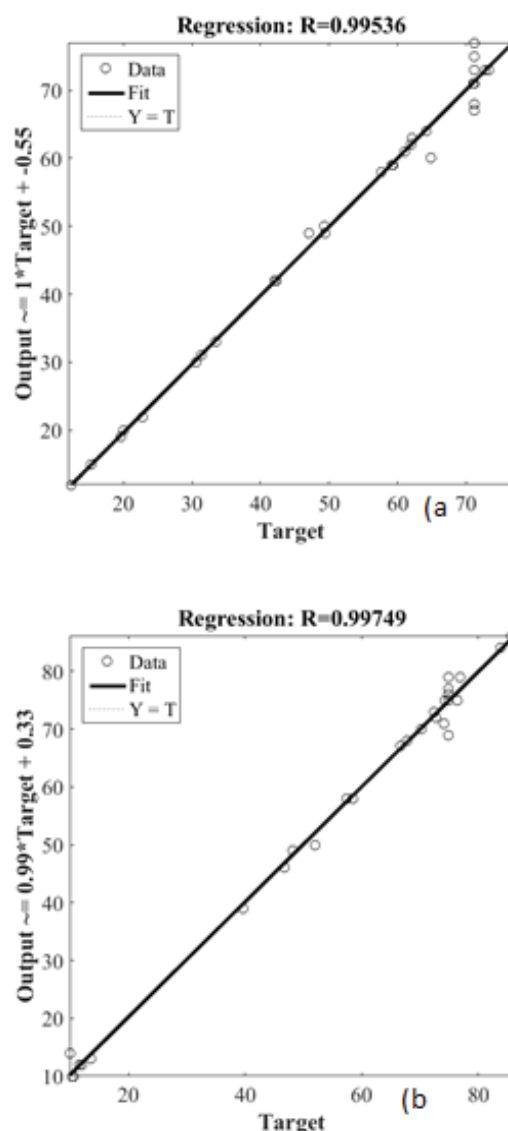


Fig. 16. The diagram of output experimental data for (a) ZnO-Syn and (b) ZnO-Fe<sub>3</sub>O<sub>4</sub>.

Table 6  
Comparison of prediction and optimization results of ANN and DOE for ZnO-Syn

Parameters	DOE	ANN
$R^2$	0.9388	0.9904
$R^2_{adj}$	0.8890	0.9881
RMSE	0.6814	0.3211
MAE	0.5211	0.2562
AAD	0.8192	0.4014

COD removal. As it can be seen in Fig. 17(a), the amount of COD removal's plot is shown in terms of oxidant and aeration rate for a constant value of 7 and 1.25 for pH and loaded catalyst, and Fig. 17(b) shows the amount of COD removal in

Table 7  
Comparison of prediction and optimization results of ANN and DOE for ZnO-Fe<sub>3</sub>O<sub>4</sub>

Parameters	DOE	ANN
R <sup>2</sup>	0.9741	0.9950
R <sub>adj</sub> <sup>2</sup>	0.9530	0.9910
RMSE	0.4421	0.2614
MAE	0.3210	0.1616
AAD	0.6071	0.3261

terms of oxidant and pH for constant value of 2.25 and 1.25 for aeration rate and loaded catalyst, and in Fig. 17(c) the amount of COD removal is shown in terms of oxidant and loaded catalyst for the constant value of 2.25 and 7 for aeration rate and pH. In general, it can be concluded from this figure that increasing the oxidant leads to increase the COD removal. According to figure, the COD removal rate is increased by increasing the aeration rate for the amount of oxidant of lesser than 220 ppm, otherwise, the COD removal is decreased by increasing the aeration rate. It can also be said, pH parameter has a periodic effect on the COD removal percentage as the following: for pH values lesser than 5.5, the COD removal

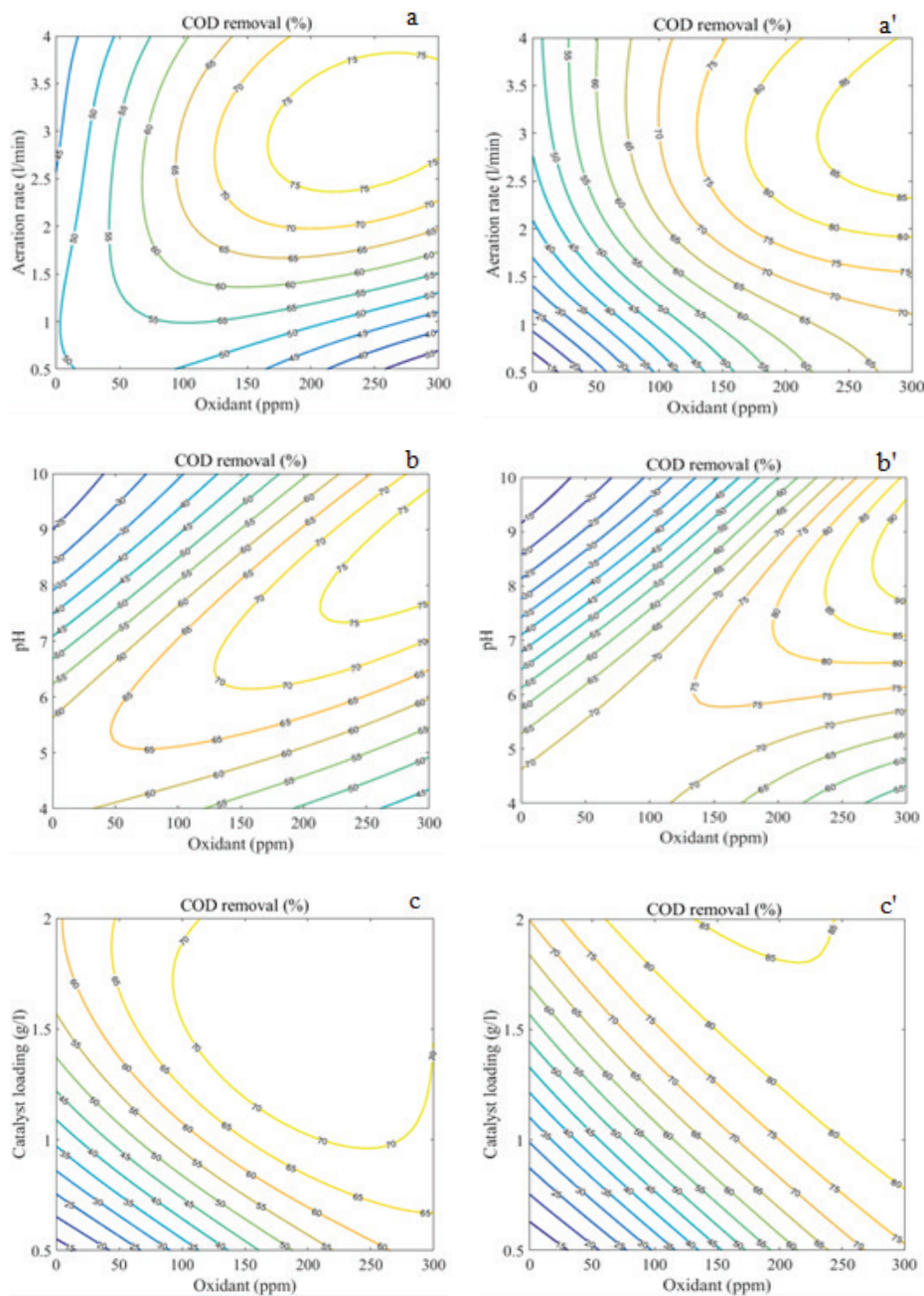


Fig. 17. Diagram of COD amount as a function of oxidizer, pH and loaded catalyst for (a)–(c) ZnO-Syn and (a')–(c') ZnO-Fe<sub>3</sub>O<sub>4</sub>.

rate is increased by increasing pH, otherwise, the COD removal rate is decreased. It can be said, the COD removal rate is increased by increasing the loaded catalyst.

### 3.5. Comparison of adsorption, photolysis and photocatalytic removal

Regular downtrend of Fig. 18 in this study demonstrates the suitability of photocatalyst treatment for this type of wastewater. In Fig. 18, the comparison among compatibles of adsorption, photolysis and photocatalyst (without factors adjustment) are provided. According to this figure, downtrend slope of ZnO-Syn catalyst is less than ZnO-Fe<sub>3</sub>O<sub>4</sub>. Also, compatibles of absorption and photolysis have negligible effect in comparison with photocatalyst compatible in COD removal efficiency.

### 3.6. Removal of existence phenol in wastewater sample

In Fig. 19, a diagram of existence phenol removal in wastewater sample is provided during the experiment by a photocatalytic process in optimized condition without limitation which shows 75% and 87% of phenol removal in the process for ZnO-Syn and ZnO-Fe<sub>3</sub>O<sub>4</sub>, respectively.

### 3.7. Removal of existence sulfide in wastewater sample

In this study, removal of existing sulfide percentage in the wastewater sample has reported for ZnO-Syn and ZnO-Fe<sub>3</sub>O<sub>4</sub>

(6.04 and 3.89 removal percentage, respectively) in 90 min and under the conditions with middle value of determined limits for factors which shows that the photocatalytic process has a negligible impact on the existing sulfide removal. But if it is assumed that the same small percentage of removal has been occurred by adsorption process, as results, it can be concluded that the photocatalytic process will not have more efficiency for the removal of inorganic compounds as sulfide.

## 4. Conclusion

In this study, spent caustic wastewater is treated by photocatalytic process. For such purpose, two type of synthesis zinc oxide (ZnO-Syn) and zinc oxide combined with Fe (ZnO-Fe<sub>3</sub>O<sub>4</sub>) photocatalyst are used separately and suspended in double wall photoreactor and reduction percentage of COD removal is determined. The result of DOE model of BBD and ANN model is in good agreement with experiment results. By comparing both models can be concluded that ANN is a better method than the DOE in predicting COD removal. The study of parameters effect of oxidizer amount, aeration rate, pH and loaded catalyst amount, alone, on COD removal, shows all parameters except pH, have a positive effect on the model. So if we do not consider the interaction effects, increasing all parameters except pH, will increase removal efficiency. Also, the interaction effect of aeration rate and photocatalyst concentration for ZnO-Syn and effect of pH and aeration rate for ZnO-Fe<sub>3</sub>O<sub>4</sub> do not exist. The study of the reciprocal effect of pH and photocatalyst in a different amount of oxidizer, indicate that high levels of oxidizer has caused a removal maintained high. Also when oxidizer is at its low level, as pH increases, removal efficiency decrease. According to provided results, it is clear the process associated with ZnO-Fe<sub>3</sub>O<sub>4</sub> catalyst has more efficient performance than the process associated with ZnO-Syn catalyst. Also, the photocatalytic method has an acceptable capability to remove the available phenol in the wastewater sample, whereas it is inefficient for the reduction of the dissolved sulfide in the wastewater.

## References

- [1] M. de Graaff, M.F.M. Bijmans, B. Abbas, G.J.W. Euverink, G. Muyzer, A.J.H. Janssen, Biological treatment of refinery spent caustics under halo-alkaline conditions, *Bioresour. Technol.*, 102 (2011) 7257–7264.
- [2] B. Kumfer, C. Felch, C. Maugans, Wet Air Oxidation Treatment of Spent Caustic in Petroleum Refineries, National Petrochemical and Refiners Association Conference, Phoenix, AZ, Vol. 23, 2010.
- [3] T.M.S. Carlos, C.B. Maugans, Wet Air Oxidation of Refinery Spent Caustic: A Refinery Case Study, NPRA Conference, San Antonio, 2000.
- [4] S.H. Sheu, H.S. Weng, Treatment of olefin plant spent caustic by combination of neutralization and Fenton reaction, *Water Res.*, 35 (2001) 2017–2021.
- [5] N. Rodriguez, H.K. Hansen, P. Nuñez, J. Guzman, Spent caustic oxidation using electro-generated Fenton's reagent in a batch reactor, *J. Environ. Sci. Health, Part A*, 43 (2008) 952–960.
- [6] P. Nuñez, H.K. Hansen, N. Rodriguez, J. Guzman, C. Gutierrez, Electrochemical generation of Fenton's reagent to treat spent caustic wastewater, *Sep. Sci. Technol.*, 44 (2009) 2223–2233.
- [7] Z.Z. Yu, D.Z. Sun, C.H. Li, P.F. Shi, X.D. Duan, G.R. Sun, J.X. Liu, UV-catalytic treatment of spent caustic from ethene plant with hydrogen peroxide and ozone oxidation, *J. Environ. Sci.*, 16 (2004) 272–275.

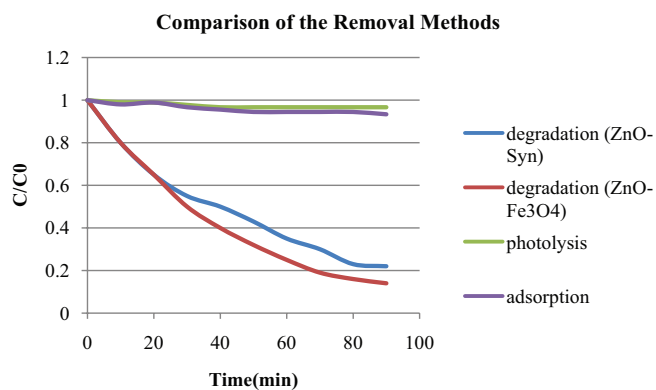


Fig. 18. Comparison of photocatalytic removal, photolysis and adsorption process.

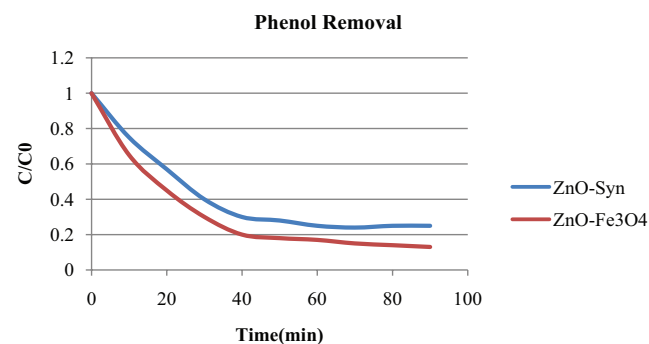


Fig. 19. Phenol photocatalytic removal.

- [8] A. Hawari, H. Ramadan, I. Abu-Reesh, M. Ouederni, A comparative study of the treatment of ethylene plant spent caustic by neutralization and classical and advanced oxidation, *J. Environ. Manage.*, 151 (2015) 105–112.
- [9] A. Shy Sayid, M.A. Abu Hassan, Z. Zainon Noor, A. Aris, Optimization of Photo-Fenton Oxidation of Sulfidic Spent Caustic By Using Response Surface Methodology, National Postgraduate Conference (NPC), 2011, pp. 1–7.
- [10] C. Chen, Wet air oxidation and catalytic wet air oxidation for refinery spent caustics degradation, *J. Chem. Soc. Pak.*, 35 (2013) 244–250.
- [11] M. Alaiezadeh, Spent Caustic Wastewater Treatment with Electrical Coagulation Method, 1st International Conference of Oil, Gas, Petrochemical and Power Plant, 2015.
- [12] R. Myers, D.C. Montgomery, C.M. Anderson-Cook, Response Surface Methodology: Process and Product Optimization Using Designed Experiments, John Wiley & Sons, Dubai, UAE, 2016.
- [13] S. Haykin, Neural Networks: A Comprehensive Foundation, Tsinghua University Press, Beijing, China, 2008.
- [14] A. Rezaee, H. Masoumbeigi, R. Darvishi, A. Khataee, S. Hashemian, Photocatalytic decolorization of methylene blue using immobilized ZnO nanoparticles prepared by solution combustion method, *Desal. Wat. Treat.*, 44 (2012) 174–179.
- [15] P. Bansal, N. Bhullar, D. Sud, Studies on photodegradation of malachite green using TiO<sub>2</sub>/ZnO photocatalyst, *Desal. Wat. Treat.*, 12 (2009) 108–113.
- [16] B. Divband, M. Khatamian, G.K. Eslamian, M. Darbandi, Synthesis of Ag/ZnO nanostructures by different methods and investigation of their photocatalytic efficiency for 4-nitrophenol degradation, *Appl. Surf. Sci.*, 284 (2013) 80–86.
- [17] Z. Wang, Novel zinc oxide nanostructures discovery by electron microscopy, *J. Phys.*, 26 (2006) 1–7.
- [18] A.Z. Khorsand, W.A. Majid, H.Z. Wang, R. Yousefi, A. Moradi Golsheikh, Z.F. Ren, Sonochemical synthesis of hierarchical ZnO nanostructures, *Ultrason. Sonochem.*, 20 (2013) 395–400.
- [19] J. Saucedo-Lucero, S. Arriaga, Photocatalytic degradation of hexane vapors in batch and continuous systems using impregnated ZnO nanoparticles, *Chem. Eng. J.*, 218 (2013) 358–367.
- [20] U. Ozgur, Y.I. Alivov, C. Liu, A. Teke, M.A. Reshchikov, S. Dogan, H. Morkoc, A comprehensive review of ZnO materials and devices, *J. Appl. Phys.*, 98 (2005) 11–19.
- [21] J. Zhu, J.X. Zhang, H.F. Zhou, W.Q. Qin, L.Y. Chai, Y.H. Hu, Microwave-assisted synthesis and characterization of ZnO-nanorod arrays, *Trans. Nonferrous Met. Soc. China*, 19 (2009) 1578–1582.
- [22] H. Smida, B. Jamoussi, Degradation of nitroaromatic pollutant by titanium dioxide/zinc phthalocyanine: study of the influencing factors, *IOSR J. Appl. Chem.*, 2 (2012) 7–11.
- [23] K.M. Kumar, B.K. Mandal, E.A. Naidu, M. Sinha, K.S. Kumar, P.S. Reddy, Synthesis and characterisation of flower shaped zinc oxide nanostructures and its antimicrobial activity, *Spectrochim. Acta, Part A*, 104 (2013) 171–174.
- [24] S. Anandan, A. Vinu, T. Mori, N. Gokulakrishnan, P. Srinivasu, V. Murugesan, K. Ariga, Photocatalytic degradation of 2,4,6-trichlorophenol using lanthanum doped ZnO in aqueous suspension, *Catal. Commun.*, 8 (2007) 1377–1382.
- [25] R. Ullah, J. Dutta, Photocatalytic degradation of organic dyes with manganese-doped ZnO nanoparticles, *J. Hazard. Mater.*, 156 (2008) 194–200.
- [26] R. Georgekutty, M.K. Seery, S.C. Pillai, A highly efficient Ag-ZnO photocatalyst: synthesis, properties, and mechanism, *J. Phys. Chem.*, 112 (2008) 13563–13570.
- [27] P. Sathishkumar, R. Sweena, J.J. Wu, S. Anandan, Synthesis of CuO-ZnO nanophotocatalyst for visible light assisted degradation of a textile dye in aqueous solution, *Chem. Eng. J.*, 171 (2011) 136–140.
- [28] M. Nikazar, M. Rostami, The optimum conditions for synthesis of Fe<sub>3</sub>O<sub>4</sub>/ZnO core/shell magnetic nanoparticles for photodegradation of phenol, *Iran. J. Environ. Health Sci. Eng.*, 12 (2014) 21–30.
- [29] D.L. Massart, B.G.M. Vandeginste, L.M.C. Buydens, S.D.E. Jong, J. Lewi, P.J. Smeyers Verbeke, Handbook of Chemometrics and Qualimetrics, Elsevier Science Inc., New York, NY, USA, 1997.
- [30] V.A. Sakkas, M.A. Islam, C. Stalikas, T.A. Albanis, Photocatalytic degradation using design of experiments: a review and example of the Congo red degradation, *J. Hazard. Mater.*, 175 (2010) 33–44.
- [31] J. Rivera-Utrilla, I. Bautista-Toledo, M.A. Ferro-García, C. Moreno-Castilla, Activated carbon surface modifications by adsorption of bacteria and their effect on aqueous lead adsorption, *J. Chem. Technol. Biotechnol.*, 76 (2001) 1209–1215.
- [32] American Public Health Association, Standard Methods for the Examination of Water and Wastewater, APHA Publication, 2005.
- [33] U.I. Gaya, A.H. Abdullah, Heterogeneous photocatalytic degradation of organic contaminants over titanium dioxide: a review of fundamentals, progress, and problems, *J. Photochem. Photobiol.*, 9 (2008) 1–12.
- [34] M. Evans, Optimization of manufacturing processes: a response surface approach, *Appl. Math. Optim. J.*, 791 (2003).
- [35] S. Nazzal, M.A. Khan, Response surface methodology for the optimization of ubiquinone self-nano emulsified drug delivery system, *AAPS Pharm. Sci. Technol.*, 3 (2002) 23–31.
- [36] D. Ranjan, D. Mishra, S.H. Hasan, Bioadsorption of arsenic: artificial neural networks and response surface methodological approach, *Ind. Eng. Chem. Res.*, 50 (2011) 9852–9863.
- [37] R. Nelofer, R.N. Ramanan, R.N. Rahman, M. Basri, A.B. Ariff, Comparison of the estimation capabilities of response surface methodology and artificial neural network for the optimization of recombinant lipase production by *E. coli* BL21, *J. Ind. Microbiol. Biotechnol.*, 39 (2012) 243–254.
- [38] M. Antonopoulou, I. Konstantinou, Photocatalytic degradation of pentachlorophenol by visible light N-F-TiO<sub>2</sub> in the presence of oxalate ions: optimization, modeling, and scavenging studies, *Environ. Sci. Pollut. Res.*, 22 (2015) 9438–9448.